Journal of Technical Science & Technologies; ISSN: 2298-0032; e-ISSN: 2346-8270; Volume 7, Issue 1, 2018

Aerodynamic Model of a Helicopter Rotating Rotor Blade

Moussa SYLLA*

Ange-Paulin Roplo BAROU**

Abstract

The aim of the present investigation is the dynamics of a rotating flexible mechanism composed of a helicopter main flexible rotor blade. In previous works of Crellin and Janssens (1983), Hablani (1982), Hughes (1974), Sylla and Barou (2008), Sylla and al (2008) neglecting the aerodynamic forces. The blade small elastic vibrations interacting with the standing rotor rotation motions are described by Rayleigh-Ritz continuum approach using the cantilever modes. In the present paper, one considers a stationary flight of the helicopter subjected to aerodynamic forces. The differential equations of the flexible blades vibrations show the interaction between the aerodynamic forces and these vibrations. The modal analysis of motions equations using Rayleigh-Ritz discretisation method leads to the blade impedance matrix spectral expansion. This matrix enables us to calculate the blade global frequencies in terms of the aerodynamic parameters.

Keywords: Impedance matrix, cantilever modes, global frequencies, aerodynamic forces.

Introduction

The spectral decomposition continuum approach of Rayleigh-Ritz Crellin and Janssens (1983), Hablani (1982), Hughes (1974), Meirovitch and Kwak (1993), Pascal (1978), (1988), (1990), (1994), Pascal and Sylla (1993), Poelaert (1981) has been used to describe the dynamics of elastic multibody systems. The cantilever modes Meirovitch and Kwak (1993), Pascal (1978), (1988), (1990), (1994), Pascal and Sylla (1993), Poelaert (1981) are generally chosen in the spectral decomposition continuum approach of Rayleigh-Ritz to perform the modal analysis of the mechanical system. The reduced impedance matrix of the multibody system derived from this analysis is obtained in terms of the cantilever modes used to describe the distributed flexibility of the mechanical system. The external torques exerted on the multibody system are related to its displacements by means of the reduced impedance matrix.

In the present paper, the spectral decomposition continuum approach of Rayleigh-Ritz is used to describe the dynamics of a flexible mechanism composed of a flexible blade of a helicopter rotor. In previous works, Pascal (1978), Pascal and Sylla (1993) neglecting the aerodynamic forces influence, this helicopter rotor was supposed to be standing and rotating with constant angular speed involving the bending, pitch and twist vibrations of the blade. Under these assumptions, the reduced impedance matrix is obtained from the modal analysis using the cantilever modes.

Here a new interest is put on the aerodynamic forces exerted on the blade. Taking into account a stationary flight of this helicopter subjected to aerodynamic forces. Thereby, the partial differential equations of the blade motions depend clearly on the aerodynamic parameters. When making use of cantilever modes in Rayleigh-Ritz discretisation theory to describe distributed flexibility in the modal analysis of these equations, one obtains the spectral expansion of the reduced impedance matrix of the elastic blade modelled as a flexible beam.

This matrix relates the blade vibrations of pitch and twist angles to an external driving force. The numerical simulations performed, establish the influence of the aerodynamic parameter on the global frequencies of vibrations in a given frequencies domain.

* Department of Mechanics and Energetics, Training and Research Unit of Mathematics and Computer Science, University Felix HOUPHOUËT-BOIGNY, 22 BP 582 Abidjan, Ivory Coast (Côte d'Ivoire).
E-mail : ba_mouss@yahoo.fr

** Department of Mechanics and Energetics, Training and Research Unit of Mathematics and Computer Science, University Felix HOUPHOUËT-BOIGNY, 22 BP 582 Abidjan, Ivory Coast (Côte d'Ivoire).
E-mail : barouange@ yahoo.fr

List of principal symbols

(B_1) - Rigid axis of the helicopter rotor

(B_2) = (O_2O) - Rigid link connecting (B_1) and (B_3)

(B_3) = (OA) - The helicopter rotor blade

P - Constant mass density of the blade (OA)

L - Length of the blade (OA)

$\vec{\Omega}_0$ - Constant angular velocity of the rotor (B_1)

E - Young modulus of the blade (OA)

$\tilde{T}$ - Axial force in the blade (OA)

(R_0) - Absolute reference frame

(B_1) - Rotating frame relative to (R_0)

(R_2) - Reference frame giving the orientation of (B_2) with respect to (R_1)

(R_3) - Reference frame giving the orientation of (B^3) with respect to (R_2)

(R) - Material reference frame connected to O

α_p, α_p^* - Circular frequencies associated with the p^{th} cantilever mode of the blade (OA)

Ω - Frequency of the global motion of the blade (OA)

f', f'' - Space derivative of the function f

$\dot{q}, \ddot{q}$ - Time derivative of the function q

Kinematics of the rotor blade

1.1 Reference frame

The blade (B_3) = (OA) is modelled by flexible beam elements of:

Length l, mass m, constant mass density ρ and Young modulus E.

The blade (B_3) is connected to rotor rigid axis (B_1) by the means of the link (B_2) = (O_2O), which is articulated on points O_2 and O, respectively with (B_1) and (B_3). The rigid link (B_2) mass is neglected and localized stiffness are introduced respectively in the joints O_2 and O. In this work, one proposes an aerodynamic model of a helicopter rotating rotor blade (figure 1). Let us denote by:

- (R_0)=(O_1 ; $\vec{x}_0$, $\vec{y}_0$, $\vec{z}_0$) is the absolute reference frame with (O_1 ; z_0) vertical axis of the rotor (B_1);
- (R_1)=(O_1 ; $\vec{x}_1$, $\vec{y}_1$, $\vec{z}_0$) is a frame rigidly connected to the rotor (B_1), rotating relative to (R_0) with constant angular velocity vector $\vec{\Omega}_0$, involving bodies (B_2) and (B_3). The frame (R_1) is deduced from (R_0) by rotation $\Psi(t)$ around (O_1 ; $\vec{z}_0$) such as:

$$\vec{\Omega}_0 = \dot{\Psi}\,\vec{z}_0, \Omega_0 = \dot{\Psi}(t); \tag{1}$$

$$\vec{y}_1 = \frac{\overrightarrow{0_1 0_2}}{a}, a = \left\|\overrightarrow{0_1 0_2}\right\|, \vec{x}_1 = \vec{y}_1 \wedge \vec{z}_0 \tag{2}$$

- (R_2)=(O_2; $\vec{x}_1$, $\vec{y}_2$, $\vec{z}_2$) is a frame connected to the link (B_2) = (O_2O) undergoing small pitch with angular velocity vector $\vec{\Omega}_1$, relative to the rotor (B_1). (R_2) is deduced from (R_1) by rotation of pitch angle $\theta(t)$ measured around (O_2; x_1) (see figure 1):

$$\vec{\Omega}_1 = \dot{\theta}(t)\vec{x}_1; \tag{3}$$

$$\vec{y}_2 = \frac{\overrightarrow{O_2O}}{b}, b = \left\|\overrightarrow{O_2O}\right\|, \ \vec{z}_2 = \vec{x}_1 \wedge \vec{y}_2; \tag{4}$$

- (R_3) = (O; $\vec{x}_3$, $\vec{y}_3$, $\vec{z}_2$) is a frame connected to the blade (B_3) to point O. One deduces the frame (R_3) from (R_2) by rotation of small twist angle $\varphi(t)$ measured around the axis (O; $\vec{z}_2$) with an angular velocity vector $\vec{\Omega}_2$:

$$\vec{\Omega}_2 = \dot{\varphi}(t)\vec{z}_2; \tag{5}$$

$$\vec{y}_3 = \frac{\overrightarrow{OA}}{l}, l = \left\|\overrightarrow{OA}\right\|, \vec{x}_3 = \vec{y}_3 \wedge \vec{z}_2; \tag{6}$$

- $(R) = (0; \vec{x}, \vec{y}, \vec{z})$ is a material reference frame rigidly connected to point O. In the undeformed configuration, the beam (OA) is lying on the axis $(0; \vec{y}_3)$ (see figure 1). One deduces the frame (R) from (R_3) by rotation of small angle $\beta(t)$ measured around the axis $(0; \vec{y}_3)$ (see figures 1 and 3) with an angular velocity vector $\vec{\Omega}_3$:

$$\vec{\Omega}_3 = \dot{\beta}(t)\vec{y}_3; \tag{7}$$

$$\vec{y} = \vec{y}_3, \ (\vec{z}_2, \vec{z}) = (\vec{x}_3 \ \ \vec{x}) = \beta(t), \ \vec{x} = \vec{y} \wedge \vec{z}. \tag{8}$$

The point $\overline{M}$ is the position of a material point M in the undeformed configuration of beam (OA). One deduces from (1), (3), (5) and (7), the frame (R) absolute angular velocity vector $\vec{\Omega}$:

$$\vec{\Omega} = \vec{\Omega}_0 + \vec{\Omega}_1 + \vec{\Omega}_2 + \vec{\Omega}_3 = \dot{\Psi}\vec{z}_0 + \dot{\theta}\vec{x}_1 + \dot{\varphi}\vec{z}_2 + \dot{\beta}\vec{y}. \tag{9}$$

The small rotations $\theta(t)$ of the rigid link (B_2)=(O_2O)

Journal of Technical Science & Technologies; ISSN: 2298-0032; e-ISSN: 2346-8270; Volume 7, Issue 1, 2018

around the axis $(O_2;\vec{x}_2)$, introduce the small displacement of the origin O, defined by the vector $\vec{r}$ expressed in the frame (R) components such that:

$$\vec{r} = \overrightarrow{O_0O} = r_1(t)\vec{x} + r_0(t)\vec{y} + r_2(t)\vec{z} \quad (10)$$

Here, O_0 is the reference position of the origin O when $\theta = 0$ (see figure 1):

$$\overrightarrow{O_2O_0} = b\vec{y}_1,\ \left\|\overrightarrow{O_2O_0}\right\| = \left\|\overrightarrow{O_2O}\right\| = b \quad (11)$$

The small elastic displacements of a material point M of the blade (OA) are represented by the vector $\vec{u}_d$, measured in the local frame (R) such that (see figure 2):

$$\vec{u}_d(s,t) = \overrightarrow{\bar{M}M} = v(s,t)\vec{x} + u(s,t)\vec{y} + w(s,t)\vec{z}. \quad (12)$$

Where $\bar{M}$ is localized by the space parameter s such that:

$$\overrightarrow{O\bar{M}} = s\vec{y};\ 0 \le s \le l = O\bar{A}; \quad (13)$$

$v(s,t)$, $w(s,t)$ are the bending deformations and $u(s,t)$ is the longitudinal deformations of the blade (OA). Since the length of the blade (OA) is not expandable during deformation, $u(s,t)$ is obtained in the form (Crellin and Janssens 1983, Pascal 1994 and Pascal and Sylla 1993);

$$u(s,t) = -\frac{1}{2}\int_0^s \left[\left(\frac{\partial v}{\partial \xi}\right)^2 + \left(\frac{\partial w}{\partial \xi}\right)^2\right] d\xi. \quad (14)$$

As consequence of (14) in the following, u are neglected in the linear theory, where r_0, r_1, r_2, v, w, θ, φ, β and their time and space derivatives are assumed to be small and of the same order. Its results from (1), the frame absolute linearized angular velocity $\vec{\Omega}$:

$$\vec{\Omega} = (\dot{\theta} - \Omega_0\beta)\vec{x} + (\dot{\beta} + \Omega_0\theta)\vec{y} + (\Omega_0 + \dot{\varphi})\vec{z} \quad (15)$$

1.2 Absolute acceleration of a material point M

The absolute position vector $\vec{X}$ of a material point M of the blade (OA) is:

$$\vec{X} = \overrightarrow{O_1M} = \overrightarrow{O_1O_0} + \overrightarrow{O_0O} + \overrightarrow{O\bar{M}} + \overrightarrow{\bar{M}M}. \quad (16)$$

Using formulas (10), (11), (12) and (13), one obtains in the frame (R) components, the absolute position vector:

$$\vec{X} = [r_1(t) + v(s,t) + l_0\cos\theta\sin\varphi\cos\beta + l_0 sin\theta\ sin\beta]\vec{x}$$
$$+[r_0(t) + u(s,t) + l_0\cos\theta\cos\varphi + s]\vec{y}$$
$$+[r_2(t) + w(s,t) + l_0\cos\theta\sin\varphi\sin\beta - l_0 sin\theta\ cos\beta]\vec{z} \quad (17)$$

Here $l_0 = a+b$. The absolute velocity vector $\vec{V}(M,t)$ of a material point M is: (18)

$$\vec{V}(M,t) = \left(\frac{d\vec{X}}{dt}\right)_{(R_0)} = \left(\frac{d\vec{X}}{dt}\right)_{(R)} + \left(\frac{d\vec{\Omega}}{dt}\right)_{(R)} \wedge \vec{X}.$$

One deduces from (18), the linearized absolute velocity vector: (19)

$$\vec{V}(M,t) = [\dot{r}_1(t) + \dot{v}(s,t) - s\dot{\varphi}(t) - \Omega_0 r_0(t) - \Omega_0(l_0 + s)]\vec{x}$$
$$+\left[\dot{r}_0(t) + \Omega_0\left(r_0(t) + v(s,t) + 2l_0\varphi(t)\right)\right]\vec{y}$$
$$+\left[\dot{r}_2(t) + \dot{w}(s,t) - s\dot{\theta}(t) + \Omega_0(l_0 + s)\beta(t)\right]\vec{z}$$

And the norm of speed vector is:

$$\left\|\vec{V}(M,t)\right\| = [\Omega_0^2(l_0 + s)^2 + 2\Omega_0^2(l_0 + s)r_0 - 2\Omega_0(l_0 +$$
$$+ s)(\dot{r}_1 + \dot{v} - s\dot{\varphi})]^{\frac{1}{2}} \quad (20)$$

It results from (16) the absolute acceleration vector $\vec{\Gamma}(M,t)$ of a material point M:

$$\vec{\Gamma}(M,t) = \left(\frac{d^2\vec{X}}{dt^2}\right)_{(R_0)} = \left(\frac{d^2\vec{X}}{dt^2}\right)_{(R)} + \left(\frac{d\vec{\Omega}}{dt}\right)_{(R)} \wedge \vec{X} +$$
$$+ 2\vec{\Omega} \wedge \left(\frac{d\vec{X}}{dt}\right)_{(R)} + \vec{\Omega} \wedge \left(\vec{\Omega} \wedge \vec{X}\right). \quad (21)$$

One deduces from (21), the linearized absolute acceleration vector $\vec{\Gamma}(M,t)$ of a material point M, in the frame (R) components:

$$\vec{\Gamma}(M,t) = \left[\ddot{r}_1(t) + \ddot{v}(s,t) - s\ddot{\varphi}(t) - 2\Omega_0\dot{r}_0(t) -\right.$$
$$\left. - \Omega_0^2\left(r_1(t) + v(s,t) + l_0\varphi(t)\right)\right]\vec{x} + \left[\ddot{r}_0(t) + 2\Omega_0\left(\dot{r}_1(t) +\right.\right.$$
$$\left.\left. + \dot{v}(s,t) - s\dot{\varphi}(t)\right) - \Omega_0^2 r_0(t) - \Omega_0^2(l_0 + s)\right]\vec{y} + \left[\ddot{r}_2(t) +\right.$$
$$\left. + \ddot{w}(s,t) + s\ddot{\theta}(t) + \Omega_0^2(l_0 + s)\theta(t)\right]\vec{z} \quad (22)$$

[Figures 1, 2, 3 and 4]

Journal of Technical Science & Technologies; ISSN: 2298-0032; e-ISSN: 2346-8270; Volume 7, Issue 1, 2018

Dynamics of the rotor blade

2.1 Aerodynamic forces

The aerodynamic forces vector $\vec{P}_a$ exerted on the rotor blade is of the form (see appendix for further details and understandings):

$$\vec{P}_a = F_{at}\vec{x} + F_{ap}\vec{z}; \tag{23}$$

where:

$$F_{at} = 0 \text{ and } F_{ap} = 4\pi R_0\rho^*\Omega_0^2(l_0+s)^2[sin(2\beta_0) + \\ + 2\beta cos(2\beta_0)]; \tag{24}$$

R_0 is the cross section radius of the blade, ρ^* is the air density and β_0 is the air rigid pitch angle with respect to the axis $(O;\vec{x}_3)$.

2.2 Local motion equations

The Euler-Bernoulli theorem developed in the work of Crellin and Janssens (1983), Wallrapp (1990), Sylla and Barou (2008) and Sylla and al (2008) is used to describe local motion of the rotor blade (OA) by taking into account the aerodynamic and gravity forces:

(25)

$$\begin{cases} \rho\begin{pmatrix}\ddot{r}_1(t)+\ddot{v}(s,t)-s\ddot{\varphi}(t)-2\Omega_0\dot{r}_0(t)-\\ -\Omega_0^2\big(r_1(t)+v(s,t)+l_0\varphi(t)\big)-g\beta(t)\end{pmatrix} \\ +EI_z\frac{\partial^4 v(s,t)}{\partial s^4}-\frac{\partial}{\partial s}\left(\tilde{T}\frac{\partial v}{\partial s}\right)=0 \\ \rho\big(\ddot{r}_2(t)+\ddot{w}(s,t)-s\ddot{\theta}(t)-\Omega_0^2(l_0+s)\theta(t)+g\big) \\ -8\pi R_0\rho^*\Omega_0^2(l_0+s)^2cos(2\beta_0)\beta(t)- \\ -4\pi R_0\rho^*\Omega_0^2(l_0+s)^2sin(2\beta_0) \\ +EI_x\frac{\partial^4 w(s,t)}{\partial s^4}-\frac{\partial}{\partial s}\left(\tilde{T}\frac{\partial w}{\partial s}\right)=0 \end{cases}$$

where $\tilde{T}(s)$ is the axial force in the blade (OA), Crellin and Janssens (1983), Pascal (1994), Sylla and Asséké (2008), Sylla and Gomat (2008), Sylla and Barou (2008) and Sylla and al (2008) (refer to appendix):

$$\tilde{T}(s) = \frac{1}{2}\rho\Omega_0^2((l_0+l)^2-(l_0+s)^2); \tag{26}$$

EI_x and EI_z are the flexural rigidity of the blade.

2.3 Global motion equations

The fundamental principle of dynamics is applied to the blade to develope global motion equations. One obtains the two following equation systems:

(27)

$$\begin{cases} m\ddot{r}_1(t)-\frac{ml}{2}\ddot{\varphi}(t)-2m\Omega_0\dot{r}_0(t)- \\ -m\Omega_0^2\big(r_1(t)+l_0\varphi(t)\big)- \\ -mg\beta(t)+\int_0^l\rho\ddot{v}(s,t)ds-\Omega_0^2\int_0^l\rho\, v(s,t)ds=F_1(t) \\ m\ddot{r}_0(t)+m\Omega_0\big(2\dot{r}_1(t)-l\dot{\varphi}(t)\big)-m\Omega_0^2r_0(t)+mg\theta(t) \\ -\frac{1}{2}m\Omega_0^2(2l_0+l)+2\Omega_0\int_0^l\rho\,\dot{v}(s,t)ds=F_2(t) \\ m\ddot{r}_2(t)+\frac{1}{2}ml\ddot{\theta}(t)+\frac{1}{2}m\Omega_0^2(2l_0+l)\theta(t) \\ -\frac{8}{3}\pi R_0\rho^*l\Omega_0^2(3l_0^2+3l_0l+l^2)cos(2\beta_0)\beta(t) \\ -\frac{4}{3}\pi R_0\rho^*l\Omega_0^2(3l_0^2+3l_0l+l^2)sin(2\beta_0)+ \\ +\int_0^l\rho\ddot{w}(s,t)ds=F_3(t) \end{cases}$$

(28)

$$\begin{cases} \frac{ml}{2}\ddot{r}_2(t)+\frac{ml^2}{3}\ddot{\theta}(t)+\frac{ml}{6}\Omega_0^2(3l_0+2l)\theta(t) \\ -\frac{1}{3}\pi R_0\rho^*l^2\Omega_0^2(6l_0^2+8l_0l+3l^2)cos(2\beta_0)\beta(t) \\ -\frac{1}{6}\pi R_0\rho^*l^2\Omega_0^2(6l_0^2+8l_0l+3l^2)sin(2\beta_0)+\frac{1}{2}mgl \\ +\int_0^l\rho s\ddot{w}(s,t)ds+\Omega_0^2\int_0^l\rho\,(l_0+s)w(s,t)ds=M_1(t) \\ \int_0^l[-\rho g+4\pi R_0\rho^*\Omega_0^2(l_0+s)^2sin(2\beta_0)]vds=M_2(t) \\ -\frac{ml}{2}\ddot{r}_1(t)+\frac{ml^2}{3}\ddot{\varphi}(t)+ml\Omega_0\dot{r}_0(t)+\frac{ml}{2}\Omega_0^2\big(r_1(t)+l_0\varphi(t)\big) \\ +\frac{1}{2}mgl\beta(t)-\int_0^l\rho s\ddot{v}(s,t)ds-l_0\Omega_0^2\int_0^l\rho\, v(s,t)ds=M_3(t) \end{cases}$$

Here $F_1(t)$, $F_2(t)$, $F_3(t)$ and $M_1(t)$, $M_2(t)$, $M_3(t)$ are respectively force and torque exerted on the rotor blade at the boundary $s = 0$.

2.4 Boundary conditions

$$\begin{cases} v(0,t)=v'(0,t)=0 \\ v''^{(l,t)}=v^{(3)}(l,t)=0 \\ F_1(t)=-EI_zv^{(3)}(0,t) \\ M_1(t)=-EI_zv''(0,t) \end{cases};\quad \begin{cases} w(0,t)=w'(0,t)=0 \\ w''^{(l,t)}=w^{(3)}(l,t)=0 \\ F_2(t)=-EI_xw^{(3)}(0,t) \\ M_2(t)=EI_xw''(0,t) \end{cases}. \tag{29}$$

Superposition methods of rayleigh-ritz

3.1 Representation of the elastic displacement

When using Rayleigh-Ritz continuum approach method, Crellin and Janssens (1983), Hughes(1974), Pascal (1994),

Journal of Technical Science & Technologies; ISSN: 2298-0032; e-ISSN: 2346-8270; Volume 7, Issue 1, 2018

Pascal and Sylla (1993), Poelaert (1981), Sylla and Barou (2008) and Sylla and al (2008) [1], [3], [8], [10], [11], [15] and [16], the elastic displacement field $v(s,t)$ and $w(s,t)$ the solutions of the equations (16), (18) and (19), are of the form:

$$\begin{cases} v(s,t) = \sum_{p=1}^{\infty} v_p(s)\lambda_p(t) \\ w(s,t) = \sum_{p=1}^{\infty} w_p(s)\lambda_p^*(t) \end{cases} \quad (30)$$

where $v_p(s)$ and $w_p(s)$ are chosen to be the cantilever modes (Crellin and Janssens 1983, Hablani 1982, Hughes 1974) of the blade (OA). λp, $\lambda^* p$ are the associated generalized coordinates. According to the previous work of Wallrapp (1990), one obtains (see appendix):

$$\begin{cases} v_p(s) = A_p\left(ch(s\mu_p) - cos(s\mu_p)\right) + \\ \quad +B_p\left(sh(s\mu_p) - sin(s\mu_p)\right) \\ w_p(s) = A_p^*\left(ch(s\mu_p^*) - cos(s\mu_p^*)\right) + \\ \quad +B_p^*\left(sh(s\mu_p^*) - sin(s\mu_p^*)\right) \end{cases} \quad (31)$$

here A_p, B_p, A^*_p and B^*_p are constants;

$$\begin{cases} \mu_p = \left(\frac{\rho}{EI_z}\right)^{\frac{1}{4}}\sqrt{\alpha_p} \\ \mu_p^* = \left(\frac{\rho}{EI_x}\right)^{\frac{1}{4}}\sqrt{\alpha_p^*} \end{cases}; \quad (32)$$

where α_p and α_p* are circular frequencies corresponding respectively to the cantilever modes $v_p(s)$ and $w_p(s)$. These cantilever modes are normalized Crellin and Janssens (1983), Hablani (1982), Pascal (1988), Wallrapp (1990) and Sylla and Barou (2008), such as:

$$\int_0^l \rho v_p v_q ds = \int_0^l \rho w_p w_q ds = \delta_{pq}; \quad \forall p, q.$$

δ_{pq} is the usual Kronecker symbol:

$$\delta_{pq} = \begin{cases} 0, & p \neq q \\ 1, & p = q \end{cases} \quad (33)$$

3.2 Determination of the generalized coordinates

The solutions of the form (30) are injected into the equations (25). Then the equations (25) are multiplied by the cantilever modes $v_p(s)$ and $w_p(s)$. When integrating these equations for $0 \leq s \leq l$ and taking into account the orthogonality property (33), one obtains;

$$\ddot{\lambda}_q + \left(\alpha_q^2 - \Omega_0^2\right)\lambda_q + \sum_{p=1}^{\infty}\tau_{pq}\lambda_p = -\rho K_m \ddot{r}_1 + 2j\rho\Omega_0 K_m \dot{r}_0 + \rho\Omega_0^2 K_m r_1 + \rho l_0 \Omega_0^2 K_m \varphi + \rho G_m \ddot{\varphi} + \rho g K_m \beta \quad (34)$$

and

$$\ddot{\lambda}^*_q + \alpha_q^{*2}\lambda_q^* + \sum_{p=1}^{\infty}\tau_{pq}^*\lambda_p^* = -\rho K_m^* \ddot{r}_2 - \rho G_m^* \ddot{\theta} - \rho\Omega_0^2(l_0 K_m^* + G_m^*)\theta + 8\pi R_0 \rho^* \Omega_0^2 cos(2\beta_0)(l_0^2 K_m^* + S_m^* + 2l_0 G_m^*)\beta + 4\pi R_0 \rho^* \Omega_0^2 sin(2\beta_0)(l_0^2 K_m^* + S_m^* + 2l_0 G_m^*) - \rho g K_m^*; \quad (35)$$

where:

$$K_q = \int_0^l v_q(s)ds;\ K_q^* = \int_0^l w_q(s)ds;$$

$$G_q = \int_0^l s v_q(s)ds;\ G_q^* = \int_0^l s w_q(s)ds;$$

$$S_q = \int_0^l s^2 v_q(s)ds;\ S_q^* = \int_0^l s^2 w_q(s)ds;$$

$$\tau_{pq} = \int_0^l \tilde{T}(s) v'_p(s) v'_q(s)ds;\ \tau_{pq}^* = \int_0^l \tilde{T}(s) w'_p(s) w'_q(s)ds. \quad (36)$$

When retaining N cantilever modes in the series of (30) and when assuming the following harmonic forms:

$$\lambda_q(t) = \hat{\lambda}_q e^{j\omega t};\ \lambda_q^*(t) = \hat{\lambda}_q^* e^{j\omega t};$$

$$\theta_q(t) = \hat{\theta}_q e^{j\omega t};\ \varphi_q(t) = \hat{\varphi}_q e^{j\omega t};\ \beta_q(t) = \hat{\beta}_q e^{j\omega t};$$

$$r_1(t) = \hat{r}_1 e^{j\omega t};\ r_0(t) = \hat{r}_0 e^{j\omega t};\ r_2(t) = \hat{r}_2 e^{j\omega t};$$

$$F_1(t) = \hat{F}_1 e^{j\omega t};\ F_2(t) = \hat{F}_2 e^{j\omega t};\ F_3(t) = \hat{F}_3 e^{j\omega t};$$

$$M_1(t) = \hat{M}_1 e^{j\omega t};\ M_2(t) = \hat{M}_2 e^{j\omega t};\ M_3(t) = \hat{M}_3 e^{j\omega t}.$$

$$j^2 = -1. \quad (37)$$

One can rewrite the equations (34) and (35) in the following forms:

$$\left[B-\left(\omega^2+\Omega_0^2\right)I\right]\hat{\lambda}=2j\rho\omega\Omega_0K\hat{r}_0+\rho\left(\omega^2+\Omega_0^2\right)K\hat{r}_1$$

$$+\rho\left(l_0\Omega_0^2K-\omega^2G\right)\bar{\varphi}+\rho gK\hat{\beta} \quad (38)$$

$$[B^*-\omega^2I]\hat{\lambda}^*=\rho\omega^2K^*\hat{r}_2+\rho\left[\omega^2G^*-\Omega_0^2(l_0K^*+G^*)\right]\hat{\theta}$$

$$+8\pi R_0\rho^*\Omega_0^2cos(2\beta_0)(l_0^2K^*+S^*+2l_0G^*)\hat{\beta}$$

$$-\rho gK^*+4\pi R_0\rho^*\Omega_0^2sin^2(\beta_0)(l_0^2K^*+S^*+2l_0G^*). \quad (39)$$

Here:

- $\hat{\lambda},\hat{\lambda}^*$ are the column matrices of the generalized coordinates of (37):

$$\hat{\lambda}=(\hat{\lambda}_1,\dots,\hat{\lambda}_N)^T;\ \hat{\lambda}^*=(\hat{\lambda}_1^*,\dots,\hat{\lambda}_N^*)^T. \quad (40)$$

- K, K^*, G, G^*, S, S^* are the column matrices of the factors (36):

$$\begin{aligned}K&=(K_1,\dots,K_N)^T;\ K^*=(K_1^*,\dots,K_N^*)^T;\\ G&=(G_1,\dots,G_N)^T;\ G^*=(G_1^*,\dots,G_N^*)^T;\\ S&=(S_1,\dots,S_N)^T;\ S^*=(S_1^*,\dots,S_N^*)^T.\end{aligned} \quad (41)$$

- B, B^* are square symmetrical matrices ($N\times N$) with respective coefficients (B_{pq}),(B^*_{pq});

$$\begin{cases}B_{pq}=\tau_{pq}+\alpha_p\alpha_q\delta_{pq}\\ B^*_{pq}=\tau^*_{pq}+\alpha^*_p\alpha^*_q\delta^*_{pq}\end{cases} \quad (42)$$

- I is the unitarian matrix (N×N) the symmetrical matrices B, B* can be diagonalized in the form of ϑ,ϑ^*by the means of the orthogonal matrices χ,χ^* from (Sylla and Asséké (2008), Sylla and Gomat (2008), Sylla and Barou (2008)) such as :

$$\begin{cases}B=\chi\vartheta\chi^T\\ B^*=\chi^*\vartheta^*\chi^{*T}.\end{cases} \quad (43)$$

Here: (44)

$$\vartheta=\begin{pmatrix}b_1&0&0&\cdots&0\\0&b_2&0&\cdots&0\\\vdots&0&\ddots&\ddots&\vdots\\0&\vdots&\ddots&\ddots&0\\0&0&\cdots&0&b_N\end{pmatrix};\ \vartheta^*=\begin{pmatrix}b_1^*&0&0&\cdots&0\\0&b_2^*&0&\cdots&0\\\vdots&0&\ddots&\ddots&\vdots\\0&\vdots&\ddots&\ddots&0\\0&0&\cdots&0&b_N^*\end{pmatrix};$$

$b_p,b_p^*(p=1,\dots,N)$ are the respective eigenvalues of the symmetrical matrices B, B^*.

- $\chi_{pq},\chi_{pq}^*(p,q=1,\dots,N)$ are respectively the coefficients of the orthogonal matrices

$$\chi,\chi^*:\chi=(\chi_{pq}),\chi^*=(\chi^*_{pq}),\qquad \chi^T\chi=\chi\chi^T=I,$$
$$\chi^{*T}\chi^*=\chi^*\chi^{*T}=I.$$

Using the diagonalization formulas (43) in equations (38) and (39) and having the following conditions (45) carried out:

$$\begin{cases}b_p\neq\omega^2+\Omega_0^2\\ b_p^*\neq\omega^{*2}\end{cases}; \quad (45)$$

one obtains the scalar generalized coordinates $\hat{\lambda}_p,\ \hat{\lambda}_p^*(p=1,\dots,N)$

(46)

$$\hat{\lambda}_p=\left[\sum_{q=1}^N\frac{\rho(\omega^2+\Omega_0^2)\chi_{pq}k_q}{b_q-(\omega^2+\Omega_0^2)}\right]\hat{r}_1+\left[\sum_{q=1}^N\frac{2j\rho\omega\Omega_0\chi_{pq}k_q}{b_q-(\omega^2+\Omega_0^2)}\right]\hat{r}_0$$
$$+\left[\sum_{q=1}^N\frac{\rho(l_0\Omega_0^2\chi_{pq}k_q-\omega^2\chi_{pq}g_q)}{b_q-(\omega^2+\Omega_0^2)}\right]\hat{\varphi}+\left[\sum_{q=1}^N\frac{\rho g\chi_{pq}k_q}{b_q-(\omega^2+\Omega_0^2)}\right]\hat{\beta}$$

and (47)

$$\hat{\lambda}_p^*=\left[\sum_{q=1}^N\frac{\rho\omega^2\chi^*_{pq}k_q^*}{b_p^*-\omega^{*2}}\right]\hat{r}_2+\left[\sum_{q=1}^N\frac{\rho\left(\left(\omega^2-\Omega_0^2\right)\chi^*_{pq}g_q^*-l_0\Omega_0^2\chi^*_{pq}k_q^*\right)}{b_p^*-\omega^{*2}}\right]\hat{\theta}$$
$$+\left[\sum_{q=1}^N\frac{8\pi R_0\rho^*\Omega_0^2cos(2\beta_0)\left(l_0^2\chi^*_{pq}k_q^*+\chi^*_{pq}s_q^*+2l_0\chi^*_{pq}g_q^*\right)}{b_p^*-\omega^{*2}}\right]\hat{\beta}$$
$$+\sum_{q=1}^N\frac{-\rho g\chi^*_{pq}k_q^*+4\pi R_0\rho^*\Omega_0^2sin(2\beta_0)\left(l_0^2\chi^*_{pq}k_q^*+\chi^*_{pq}s_q^*+2l_0\chi^*_{pq}g_q^*\right)}{b_p^*-\omega^{*2}}$$

here:

$$k=\chi^TK=(k_1,\dots,k_N)^T,k_p=\sum_{q=1}^N\chi_{qp}K_q;k^*=\chi^{*T}K^*=$$
$$=(k_1^*,\dots,k_N^*)^T;\ k_q^*=\sum_{q=1}^N\chi^*_{qp}K_q^*;$$

$$\mathrm{g}=\chi^TG=(\mathrm{g}_1,\dots,\mathrm{g}_N)^T,\mathrm{g}_p=\sum_{q=1}^N\chi_{qp}G_q;\mathrm{g}^*=\chi^{*T}G^*=$$
$$=(\mathrm{g}_1^*,\dots,\mathrm{g}_N^*)^T;\ \mathrm{g}_q^*=\sum_{q=1}^N\chi^*_{qp}G_q^*;$$

$$s=\chi^TS=(s_1,\dots,s_N)^T,s_p=\sum_{q=1}^N\chi_{qp}S_q;s^*=\chi^{*T}S^*=$$

Journal of Technical Science & Technologies; ISSN: 2298-0032; e-ISSN: 2346-8270; Volume 7, Issue 1, 2018

$$= (s_1^*, \dots, s_N^*)^T;\ s_q^* = \sum_{q=1}^{N} \chi_{qp}^* S_q^*;$$

K_q, G_q, S_q, K_p^*, G_p^* and S_p^* are obtained from formulas (36).

3.3 Derivation of the impedance matrices

The two bending vibration motions *v(s,t)* and *w(s,t)* are coupled contrary to the works of Sylla and Barou (2008) and Sylla and al (2008). The global motion equations (18) and (19) can be transformed by using the discretization (30) of displacements *v(s,t)* and *w(s,t)*, the harmonic forms (37), formulas (46), (47) and scalars generalized coordinates $\hat{\lambda}_p$ and $\hat{\lambda}_p^*$. One obtains finally (see appendix):

$$Z(\omega)\bar{R} = \bar{Q} \tag{48}$$

where:

- $\bar{R}$, $\bar{Q}$ column matrices of displacements and forces respectively : (49)

$$\hat{R} = \left(\hat{r}_1, \hat{r}_0, \hat{r}_2, \hat{\theta}, \hat{\varphi}, \hat{\beta}\right)^T, \qquad \hat{Q} = \left(\hat{F}_1, \hat{F}_2, \hat{F}_3, \hat{M}_1, \hat{M}_2, \hat{M}_3\right)$$

- *Z(ω)* the reduced impedance matrix of the rotor blade *(OA)*. *Z* is given by a spectral expansion in terms of the cantilever modes (Crellin and Janssens 1983, Hablani 1982, Hughes 1974, Pascal 1988, 1990, 1994, Pascal and Sylla 1993 Sylla and Asséké 2008 and Sylla and Barou 2008):

$$\mathrm{Z}(\omega) = Z_0 + \sum_{q=1}^{N} Z_q \tag{50}$$

$$Z_0 = Z_0^R + jZ_0^I;\ \text{with } j^2 = -1 \tag{51}$$

where:

$$Z_0^R = \begin{pmatrix} G_{11}^R & 0 & 0 & 0 & G_{15}^R & G_{16}^R \\ 0 & G_{22}^R & 0 & G_{24}^R & 0 & 0 \\ 0 & 0 & G_{33}^R & G_{34}^R & 0 & G_{36}^R \\ 0 & 0 & G_{43}^R & G_{44}^R & 0 & G_{46}^R \\ 0 & 0 & 0 & 0 & 0 & 0 \\ G_{61}^R & 0 & 0 & 0 & G_{65}^R & G_{66}^R \end{pmatrix}; \tag{52}$$

and:

$$Z_0^I = \begin{pmatrix} 0 & 0 & 0 & 0 & 0 & 0 \\ G_{21}^I & 0 & 0 & 0 & G_{25}^I & 0 \\ 0 & 0 & 0 & 0 & 0 & 0 \\ 0 & 0 & 0 & 0 & 0 & 0 \\ 0 & 0 & 0 & 0 & 0 & 0 \\ 0 & G_{62}^I & 0 & 0 & 0 & 0 \end{pmatrix}; \tag{53}$$

One also obtains;

$$Z_q = Z_p^R + jZ_q^I \quad \text{with} \quad j^2 = -1 \tag{54}$$

where

$$Z_q^R = \begin{pmatrix} V_{11}^R & 0 & 0 & 0 & V_{15}^R & V_{16}^R \\ 0 & V_{22}^R & 0 & 0 & 0 & 0 \\ 0 & 0 & V_{33}^R & V_{34}^R & 0 & 0 \\ 0 & 0 & V_{43}^R & V_{44}^R & 0 & V_{46}^R \\ V_{51}^R & 0 & 0 & 0 & V_{55}^R & V_{56}^R \\ V_{61}^R & 0 & 0 & 0 & V_{65}^R & V_{66}^R \end{pmatrix}; \tag{55}$$

and

$$Z_q^I = \begin{pmatrix} 0 & V_{12}^I & 0 & 0 & 0 & 0 \\ V_{21}^I & 0 & 0 & 0 & V_{25}^I & V_{26}^I \\ 0 & 0 & 0 & 0 & 0 & 0 \\ 0 & 0 & 0 & 0 & 0 & 0 \\ 0 & V_{52}^I & 0 & 0 & 0 & 0 \\ 0 & V_{62}^I & 0 & 0 & 0 & 0 \end{pmatrix}; \tag{56}$$

the coefficients of the matrix Z are (see appendix):

$$G_{11}^R = -\rho l\left(\Omega_0^2 + \omega^2\right);\ G_{22}^R = -\rho l\left(\Omega_0^2 + \omega^2\right);$$

$$G_{15}^R = \frac{1}{2}\rho l\left(l\omega^2 - 2l_0\Omega_0^2\right);\ G_{24}^R = \rho g l;\ G_{33}^R = -\rho l\omega^2;$$

$$G_{16}^R = -\rho g l;\ G_{34}^R = \frac{1}{2}\rho l\left(l\omega^2 + \Omega_0^2(2l_0 + l)\right);$$

$$G_{36}^R = -\frac{8}{3}\pi R_0\rho^*\Omega_0^2 cos(2\beta_0)l(3l_0^2 + 3l_0 l + l^2);\ G_{43}^R =$$

$$= -\frac{1}{2}\rho l^2\omega^2;$$

$$G_{44}^R = \frac{1}{6}\rho l^2\left((3l_0 + 2l)\Omega_0^2 - 2\omega^2\right);\ G_{46}^R =$$

$$= -\frac{2}{3}\pi R_0\rho^* l^2\Omega_0^2 cos(2\beta_0)(6l_0^2 + 8l_0 l + 3l^2);$$

$$G_{61}^R = \frac{1}{2}\rho l^2\left(\Omega_0^2 + \omega^2\right);$$

$$G_{65}^R = \frac{1}{6}\rho l^2\left(3l_0\Omega_0^2 - 2l\omega^2\right);\ G_{66}^R = \frac{1}{2}\rho g l^2.$$

$$G_{21}^I = 2\rho l\omega\Omega_0;\ G_{25}^I = -\rho l^2\omega\Omega_0;\ G_{62}^I = \rho l^2\omega\Omega_0;$$

$$V_{11}^R = -\rho\left(\Omega_0^2 + \omega^2\right)\left[\frac{\rho\left(\Omega_0^2 + \omega^2\right)k_q^2}{b_q - \left(\Omega_0^2 + \omega^2\right)}\right];$$

Journal of Technical Science & Technologies; ISSN: 2298-0032; e-ISSN: 2346-8270; Volume 7, Issue 1, 2018

$$V_{15}^{R} = -\rho^2\left(\Omega_0^2 + \omega^2\right)\left[\frac{l_0\Omega_0^2 k_q^2 - \omega^2 k_q \mathrm{g}_q}{b_q - \left(\Omega_0^2 + \omega^2\right)}\right];$$

$$V_{16}^{R} = -\rho\left(\Omega_0^2 + \omega^2\right)\left[\frac{\rho \mathrm{g} k_q^2}{b_q - \left(\omega^2 + \Omega_0^2\right)}\right];$$

$$V_{22}^{R} = -\frac{(2\rho\omega\Omega_0)^2 k_q^2}{b_q - \left(\Omega_0^2 + \omega^2\right)};$$

$$V_{33}^{R} = -\frac{\left(\rho\omega^2 k_q^*\right)^2}{b_q^* - \omega^2};$$

$$V_{34}^{R} = -\rho^2\omega^2\left[\frac{\left(\Omega_0^2 + \omega^2\right)k_q^* \mathrm{g}_q^* - l_0\Omega_0^2 k_q^{*2}}{b_q^* - \omega^2}\right];$$

$$V_{36}^{R} = -8\pi R_0\rho^*\rho\omega^2\Omega_0^2 cos(2\beta_0)\left[\frac{\left(l_0^2 k_q^{*2} + k_q^* s_q^* + 2l_0 k_q^* \mathrm{g}_q^*\right)}{b_q^* - \omega^2}\right];$$

$$V_{43}^{R} = \rho^2\omega^2\left[\frac{l_0\Omega_0^2 k_q^{*2} + \left(\Omega_0^2 - \omega^2\right)k_q^* \mathrm{g}_q^*}{b_q^* - \omega^2}\right];$$

$$V_{44}^{R} = \rho^2\left[\frac{\left(l_0\Omega_0^2 k_q^* + \left(\Omega_0^2 - \omega^2\right)\mathrm{g}_q^*\right)^2}{b_q^* - \omega^2}\right];$$

$$V_{46}^{R} = 8\pi R_0\rho^*\rho\Omega_0^2 cos(2\beta_0)\left[\frac{l_0^3\Omega_0^2 k_q^{*2} + 2l_0\left(\Omega_0^2 - \omega^2\right)\mathrm{g}_q^{*2}}{b_q^* - \omega^2} + \frac{l_0^2\left(3\Omega_0^2 - \omega^2\right)k_q^* \mathrm{g}_q^* + l_0\Omega_0^2 k_q^* s_q^* + \left(\Omega_0^2 - \omega^2\right)\mathrm{g}_q^* s_q^*}{b_q^* - \omega^2}\right];$$

$$V_{51}^{R} = \rho\left(\Omega_0^2 + \omega^2\right)\left[\frac{\left(-\rho\mathrm{g} + 4\pi R_0\rho^* l_0^2\Omega_0^2 sin(2\beta_0)\right)k_q^2 + 4\pi R_0\rho^*\Omega_0^2 sin(2\beta_0)\left(2l_0 k_q \mathrm{g}_q + k_q \mathrm{s}_q\right)}{b_q - \left(\Omega_0^2 + \omega^2\right)}\right];$$

$$V_{55}^{R} = \rho\left[\frac{l_0\Omega_0^2\left(-\rho\mathrm{g} + 4\pi R_0\rho^* l_0^2\Omega_0^2 sin(2\beta_0)\right)k_q^2 - 8\pi R_0\rho^* l_0\Omega_0^2\omega^2 sin(2\beta_0)\mathrm{g}_q^2}{b_q - \left(\Omega_0^2 + \omega^2\right)}\right.$$

$$+\frac{\left(\rho\mathrm{g}\omega^2 + 4\pi R_0\rho^* l_0^2\Omega_0^2\left(2\Omega_0^2 - \omega^2\right)sin(2\beta_0)\right)k_q \mathrm{g}_q}{b_q - \left(\Omega_0^2 + \omega^2\right)}$$

$$\left.+\frac{4\pi R_0\rho^*\Omega_0^2 sin(2\beta_0)\left(l_0\Omega_0^2 k_q \mathrm{s}_q - \omega^2 \mathrm{g}_q \mathrm{s}_q\right)}{b_q - \left(\Omega_0^2 + \omega^2\right)}\right];$$

Journal of Technical Science & Technologies; ISSN: 2298-0032; e-ISSN: 2346-8270; Volume 7, Issue 1, 2018

$$V_{55}^{R} = \rho\left[\frac{l_0\Omega_0^2\left(-\rho g + 4\pi R_0\rho^* l_0^2\Omega_0^2 sin(2\beta_0)\right)k_q^2 - 8\pi R_0\rho^* l_0\Omega_0^2\omega^2 sin(2\beta_0)g_q^2}{b_q - \left(\Omega_0^2+\omega^2\right)}\right.$$

$$\left. + \frac{\left(\rho g\omega^2 + 4\pi R_0\rho^* l_0^2\Omega_0^2\left(2\Omega_0^2-\omega^2\right)sin(2\beta_0)\right)k_q g_q}{b_q - \left(\Omega_0^2+\omega^2\right)} + \frac{4\pi R_0\rho^*\Omega_0^2 sin(2\beta_0)\left(l_0\Omega_0^2 k_q s_q - \omega^2 g_q s_q\right)}{b_q - \left(\Omega_0^2+\omega^2\right)}\right];$$

$$V_{56}^{R} = \rho g\left[\frac{\left(-\rho g + 4\pi R_0\rho^* l_0^2\Omega_0^2 sin(2\beta_0)\right)k_q^2 + 2\pi R_0\rho^*\Omega_0^2 sin(2\beta_0)\left(2l_0 k_q g_q + k_q s_q\right)}{b_q - \left(\Omega_0^2+\omega^2\right)}\right];$$

$$V_{61}^{R} = -\rho^2\left(\Omega_0^2+\omega^2\right)\left[\frac{l_0\Omega_0^2 k_q^2 - \omega^2 k_q g_q}{b_q - \left(\Omega_0^2+\omega^2\right)}\right];$$

$$V_{65}^{R} = -\rho^2\left[\frac{\left(l_0\Omega_0^2 k_q - \omega^2 g_q\right)^2}{b_q - \left(\Omega_0^2+\omega^2\right)}\right];$$

$$V_{66}^{R} = \rho^2 g\left[\frac{l_0\Omega_0^2 k_q^2 - \omega^2 k_q g_q}{b_q - \left(\Omega_0^2+\omega^2\right)}\right].$$

$$V_{12}^{I} = -2\rho^2\omega\Omega_0\left[\frac{\left(\Omega_0^2+\omega^2\right)k_q^2}{b_q - \left(\Omega_0^2+\omega^2\right)}\right];$$

$$V_{21}^{I} = 2\rho^2\omega\Omega_0\left[\frac{\left(\Omega_0^2+\omega^2\right)k_q^2}{b_q - \left(\Omega_0^2+\omega^2\right)}\right];$$

$$V_{25}^{I} = 2\rho^2\omega\Omega_0\left[\frac{l_0\Omega_0^2 k_q^2 - \omega^2 k_q g_q}{b_q - \left(\Omega_0^2+\omega^2\right)}\right];$$

$$V_{26}^{I} = 2\rho\omega\Omega_0\left[\frac{\rho g k_q^2}{b_q - \left(\omega^2+\Omega_0^2\right)}\right];$$

$$V_{52}^{I} = 2\rho\omega\Omega_0\left[\frac{\left(-\rho g + 4\pi R_0\rho^* l_0^2\Omega_0^2 sin(2\beta_0)\right)k_q^2}{b_q - \left(\Omega_0^2+\omega^2\right)} + \frac{4\pi R_0\rho^*\Omega_0^2 sin(2\beta_0)\left(2l_0 k_q g_q + k_q s_q\right)}{b_q - \left(\Omega_0^2+\omega^2\right)}\right];$$

$$V_{62}^{I} = -2\rho^2\omega\Omega_0\left[\frac{l_0\Omega_0^2 k_q^2 - \omega^2 k_q g_q}{b_q - \left(\Omega_0^2+\omega^2\right)}\right].$$

The global frequencies $\omega q\ (q = 1, \ldots, \infty)$ of the bending vibration modes $v(s,t)$ and $w(s,t)$ are the roots of the impedance matrix Z such that:

$$detZ(\omega_q) = 0, \quad q = 1, \ldots, \infty$$

Numerical simulations

The simulations are done with the following data, Wallrapp (1990):

$$l = 4m;\ \rho = 13.935\ kg/m;\ a = 0.6\ m;\ b = 0.2\ m;$$

$$b = 0.2\ m;\ EI_x = EI_z = 1.9\times10^4 Nm^2,\ m = 55.74\ kg.$$

Since the flexural rigidity EI_x and EI_z are identical, the two cantilever bending modes $v_p(s)$ and $w_p(s)$ are the same (see formulas (36)):

$$EI_x = EI_z \Rightarrow v_p(s) = w_p(s).$$

It results that the circular frequencies α_p, α_p^* corresponding respectively to $v_p(s)$ and $w_p(s)$ are identical: $\alpha_p = \alpha_p^*$.

A numerical program computes the cantilever bending frequencies α_p in Table 1.

The cantilever bending frequencies α_p are used by a numerical program to compute the global frequencies ω_p (Figures 5).

Figures 5 show that the global modes have certain values of frequencies in common. One deduces the behavior from the first frequency cantilever among the values of total frequencies (see Figure 6).

With $\beta_0 = 0.01°$, the first cantilever frequency preserves its values for angular velocity values from 0 to 3 rad/s and gives a rise to two other frequencies of $\Omega_0 = 1$ rad/s. One of these frequencies follows a decreasing parabolic function from $\omega_1 = 1.28\ Hz$ for $\Omega_0 = 1\ rad/s$ to $\omega_1 = 0.2\ Hz$ for $\Omega_0 = 8\ rad/s$. The other frequency with an increasing quasi linear evolution of $\omega_1 = 1.31\ Hz$ for $\Omega_0 = 1\ rad/s$ to $\omega_1 = 2.92\ Hz$ for $\Omega_0 = 18\ rad/s$.

While $\beta_0 = 5°$, the cantilever frequency follows two evolutions, one constant and the other decreasing parabolic function, identical to those obtained in $\beta_0 = 0.01°$.

Referring to these results it can be said that, taking into account aerodynamic forces in the dynamic modeling of a helicopter blade in stationary flight, it revealed new vibration frequencies, which are absent in the previous studies.

And one observes the presence of cantilever frequencies, among the global frequencies of the system, for each given value of angular speed.

Conclusion

The aerodynamic model presented in this work complete the modeling by continuum approach of a rotating rotor blade of a helicopter which supposed to be standing, carried out in the previous works of Sylla and Barou (2008) and Sylla and al (2008). The motion equations are elaborates when taking into account the aerodynamic and gravity forces exerted on a rotor blade of a helicopter in stationary flight.

The spectral development of the impedance matrix showed the presence of the cantilever frequencies among the obtained numerically global frequencies obtained, for each angular speed value. The influence of the pitch and twist angles on the elastic behavior of the rotor blade is also observed.

References

Crellin E. and Janssens F. 1983. Derivation and Combinations of Impedance Matrices for Flexible Satellites, European Space Agency/ ESA STR-209.

Hablani H. B. 1982. Modal Analysis of Gyroscopic Flexible Spacecraft: A Continuum Approach, AIAA Journal, 5(3), pp. 448-457.

Hughes P. C. 1974. Dynamics of Flexible Space Vehicles with Active Attitudes Control, Celestial Mechanics, 9.

Meirovitch L., Stationarity A. 1976. Principle for the Eigenvalue Problem for Rotating Structures, AIAA Journal, 14(10), pp.1387-1394.

Meirovitch L. and Kwak M. K. 1993. Rayleigh-Ritz Based structure Synthesis for Flexible Satellite European Space Agency/ ESA STR-209.

P. Germain, P. Muller 1995. Introduction à la mécanique des milieux continus, 2ème édition. Pascal M. 1978. La stabilité d'Attitude d'un Satellite muni de Panneaux Solaires, Acta Astronautica, 5, pp.817-844.

Pascal M. 1988. Dynamics Analysis of a System of Hinge Connected Flexible Bodies, Celestial Mechanics, 41, pp. 21-39.

Pascal M. 1990. Dynamical Analysis of a Manipulator Arm, Acta Astronautica, 21(3), pp.161-169.

Pascal M. 1994. Modal Analysis of a Rotating Flexible Space Station by a Continuous Approach, Z. Flugwiss Weltraumforsch, 18, pp.385-401.

Pascal M. and Sylla M. 1993. Dynamics Model of a Large

Journal of Technical Science & Technologies; ISSN: 2298-0032; e-ISSN: 2346-8270; Volume 7, Issue 1, 2018

Space Structure by continuous Approach, Recherche Aérospatiale 1993(2), pp. 67-77.

Poelaert D. 1981. Spacecraft Dynamics Analysis using Cantilever Modes of the Appendages - Application to the Space Telescope, ESA STR 206.

Servera G. 2002. Développement d'une méthodologie de couplage dynamique/aérodynamique pour les rotors d'hélicoptère.

Sylla M. and Asséké B. 2008. Dynamics of a Rotating Flexible and Symmetric Spacecraft using Impedance Matrix in terms of the flexible Appendages cantilever Modes, European Journal of Multibody System Dynamics, 19, pp. 345-364.

Sylla M. and Gomat L. 2008. Modal Analysis of a Rotating Flexible Manipulator Arm, Journal de l'Union Mathematique Africaine, AfrikaMatematika, 19(3), pp. 7-28.

Sylla M. and Barou R. 2008. A Mathematical Model of a Helicopter Standing and Rotating Rotor Blade, Far East Journal of Applied Mathematics, 31(1), pp.1-25.

Sylla M., Dosso M., Barou R. 2008. Dynamical Analysis of a Flexible Mechanism by a Continuum Approach using the Rotating Base Cantilever Modes, Far East Journal of Applied Mathematics, 33(2), pp.187-204.

Wallrapp O., Santos J. and Ryu J. 1990. Superposition Method for Stress Stiffening in Flexible Multibody Dynamics, Proc. Int. Conf. on Dynamics of Flexible Structures on Space, Cranfield, UK, pp.233-247, CMP&Springer-Verlag.

Appendix

Aerodynamic forces

The theory of irrotationnel and stationary plan flow of incompressible perfect fluid around an obstacle P. Germain, P. Muller (1995) is used to model the aerodynamic forces (Figure 7).

The cross section of the blade is considered as a circle and the complex velocity of a fluid (in this case air) around a circle is, P. Germain, P. Muller (1995) and Servera (2002):

$$\zeta = V^*\left(e^{-j\beta^*} - \frac{e^{j\beta^*}}{Z^2}\right) + \frac{j\Gamma^*}{2\pi}\frac{1}{Z};$$

here V^* and β^* are respectively winds speed and incident angle (relative to x_3 axis), Γ^* is the air circulation around the circle of radius R_0.

Any circle point was spotted by the complex number Z such as:

$$Z = R_0 e^{j\theta^*} \text{ with } j^2 = -1 \text{ and } \theta^* \in [0; 2\pi].$$

According to the Kutta-Juckosky condition, P. Germain, P. Muller (1995) and Servera (2002), velocity to the trailing edge ($\theta^*=0$) should be finite, which implies:

$$\Gamma^* = 4\pi R_0 V^* sin(\beta^*).$$

Therefore the air velocity around the circle is:

$$\|\zeta\| = V = 2V^*\big(\sin(\theta^* - \beta^*) + \sin(\beta^*)\big).$$

By applying Bernoulli theorem in the absence of fluid volume forces, it comes;

$$P_e - P_i = 2\rho^* V^{*2}\sin(2\beta^*)[\sin(2\theta^*) - 2\sin(\theta^*)];$$

where, P_e and P_i are respectively the pressure exerted by the air in extrados $(\theta^* \in [0;\pi])$ and in intrados $(\theta^* \in [\pi;2\pi])$ of the cross section and ρ^* is the air density. It is the difference between these two pressures that arise aerodynamic forces on a circular section (Figure 8).

They are defined as follows:

$$F_{at} = \int_0^{2\pi} (P_e - P_i)cos(\theta^*)d\theta^*$$

and

$$F_{ap} = \int_0^{2\pi} (P_e - P_i)sin(\theta^*)d\theta^*;$$

where F_{at}, F_{ap} are respectively the drag and lift aerodynamic forces density (see Figure 8).

Moreover, in this study, we suppose that the incident velocity of the air with respect to the blade is:

$$V^{*2} = \Omega_0^2(l_0 + s)^2;$$

Because the influence of motion parameters is neglected before the angular velocity Ω_0. And, the incident angle of the air with respect to axis $(O, \vec{x}_3)$ is written as follows:

$$\beta^* = \beta_0 + \beta(t);$$

Where β_0 is the rigid incidence angle of the air with respect to the axis $(O, \vec{x}_3)$ and $\beta(t)$ which represent the pitch angle and the motion parameter. It leads to:

Journal of Technical Science & Technologies; ISSN: 2298-0032; e-ISSN: 2346-8270; Volume 7, Issue 1, 2018

Local motions of the rotor blade (OA)

The local motion of the rotor blade (OA) is governed by the dynamics fundamental equations, Crellin and Janssens (1983):

$$\begin{cases} \frac{d\vec{F}(s,t)}{ds} + \rho\vec{g} + \vec{P}_a = \rho\frac{d^2\vec{X}(s,t)}{ds^2} & \text{(a1.1)} \\ \frac{d\vec{M}(s,t)}{ds} + \frac{d\vec{X}(s,t)}{ds} \wedge \vec{F}(s,t) = \vec{0} & \text{(a1.2)} \end{cases}$$

where $\vec{F}, \vec{M}$ are respectively the force and torque exerted into the rotor blade *(OA)*, of components in frame *(R)*:

$$\vec{F} = \left(F_x(s,t) + \tilde{T}_1(s); F_y(s,t) + \tilde{T}_2(s); F_z(s,t) + \tilde{T}_3(s)\right), \quad \text{(a.2)}$$

$$\vec{M} = (m_x; 0; m_z); \quad \text{(a.3)}$$

Let's recall that $\overrightarrow{X}$ is the position vector of a material point M of the rotor blade *(OA)*, given by formulas (16), $\rho\vec{g}$ and $\vec{P}_a$ which are respectively the gravity and aerodynamic forces vectors exerted on the rotor blade. Formula (a.1.1) becomes:

$$\frac{d\vec{F}(s,t)}{ds} + \rho\vec{g} + \vec{P}_a \begin{pmatrix} 0 \\ 0 \\ 4\pi R_0\rho^*\Omega_0^2(l_0+s)^2\left(sin(2\beta_0) + 2\beta cos(2\beta_0)\right) \end{pmatrix} = \rho\vec{\Gamma}(M,t) \quad \text{(a.4)}$$

$$= \rho \begin{pmatrix} \ddot{r}_1 + \ddot{v} - s\ddot{\varphi} - 2\Omega_0\dot{r}_0 - \Omega_0^2(r_1 + v + l_0\varphi) \\ \ddot{r}_0 + 2\Omega_0(\dot{r}_1 + \dot{v} - s\dot{\varphi}) - \Omega_0^2 r_0 - \Omega_0^2(l_0 + s) \\ \ddot{r}_2 + \ddot{w} + s\ddot{\theta} + \Omega_0^2(l_0 + s)\theta \end{pmatrix}$$

One obtains components of the axial force vector:

$$\tilde{T}_1(s) = 0;$$

$$\tilde{T}_2(s) = \tilde{T}(s) = -\frac{1}{2}\rho\Omega_0^2[(l_0+s)^2 - (l_0+l)^2] \quad \text{(a.5)}$$

and

$$\tilde{T}_3(s) = \rho g(s-l) - \frac{4}{3}\pi R_0\rho^*\Omega_0^2[(l_0+s)^3 - (l_0+l)^3]sin(2\beta_0)$$

One assumes Euler-Bernoulli beam for the rotor blade (OA). So that

$$m_x = EI_x\frac{\partial^2 w}{\partial s^2};\ \ m_z = -EI_z\frac{\partial^2 v}{\partial s^2}. \quad \text{(a.6)}$$

By derivating equation (a.1.2) with respect to the variables, one obtains:

$$\frac{d^2\vec{M}(s,t)}{ds^2} + \frac{d^2\vec{X}(s,t)}{ds^2} \wedge \vec{F}(s,t) + \frac{d\vec{X}(s,t)}{ds} \wedge \frac{d\vec{F}(s,t)}{ds} = \vec{0}$$

It results from the last equation combined with (a.2), (a.3) and formulas (a.4), (a.6), the linearized equations of the rotor blade (OA) local motion:

$$\rho\left(\ddot{r}_1(t) + \ddot{v}(s,t) - s\ddot{\varphi}(t) - 2\Omega_0\dot{r}_0(t) - \Omega_0^2\left(r_1(t) + v(s,t) + l_0\varphi(t)\right) - g\beta(t)\right) + EI_z\frac{\partial^4 v(s,t)}{\partial s^4} - \frac{\partial}{\partial s}\left(\tilde{T}\frac{\partial v}{\partial s}\right) = 0 \quad \text{(a.7)}$$

$$\rho\left(\ddot{r}_2(t) + \ddot{w}(s,t) - s\ddot{\theta}(t) - \Omega_0^2(l_0+s)\theta(t) + g\right) - 8\pi R_0\rho^*\Omega_0^2(l_0+s)^2 cos(2\beta_0)\beta(t) - 4\pi R_0\rho^*\Omega_0^2(l_0+s)^2 sin(2\beta_0) + EI_x\frac{\partial^4 w(s,t)}{\partial s^4} - \frac{\partial}{\partial s}\left(\tilde{T}\frac{\partial w}{\partial s}\right) = 0 \quad \text{(a.8)}$$

[Table 2]; [Figures 9 and 10]

Journal of Technical Science & Technologies; ISSN: 2298-0032; e-ISSN: 2346-8270; Volume 7, Issue 1, 2018

Tables

Table 1. $\Omega_0=0$ rad/s, cantilever bending frequencies

$\frac{\alpha_p}{2\pi}$ (Hz) [0-340Hz]			
1.2914	44.4075	153.1616	327.1677
8.0993	73.4088	203.9134	
22.6615	109.660	261.9161	

Table 2. Values of ω the global frequency when Ω_0 tends towards 0 rad/s

	$\beta_0 = 0.01°, -3, -5°, 5°, 10°$			
	$10^{-7}\ rad/s$	$10^{-6}\ rad/s$	$10^{-5}\ rad/s$	$10^{-4}\ rad/s$
$\frac{\omega_p}{2\pi}$ (Hz)	1.29114448	1.29114448	1.29114448	1.29114448
	8.09103942	8.09103942	8.09103942	8.09103942
	22.6547114	22.6547114	22.6547114	22.6547114
	44.4062186	44.4062186	44.4062186	44.4062186
	73.4062386	73.4062386	73.4062386	73.4062386
	109.659745	109.659745	109.659745	109.659745
	153.158781	153.158781	153.158781	153.158781
	203.911303	203.911303	203.911303	203.911303
	261.911343	261.911343	261.911343	261.847681
	327.164869	327.164869	327.164869	327.213611

Figures

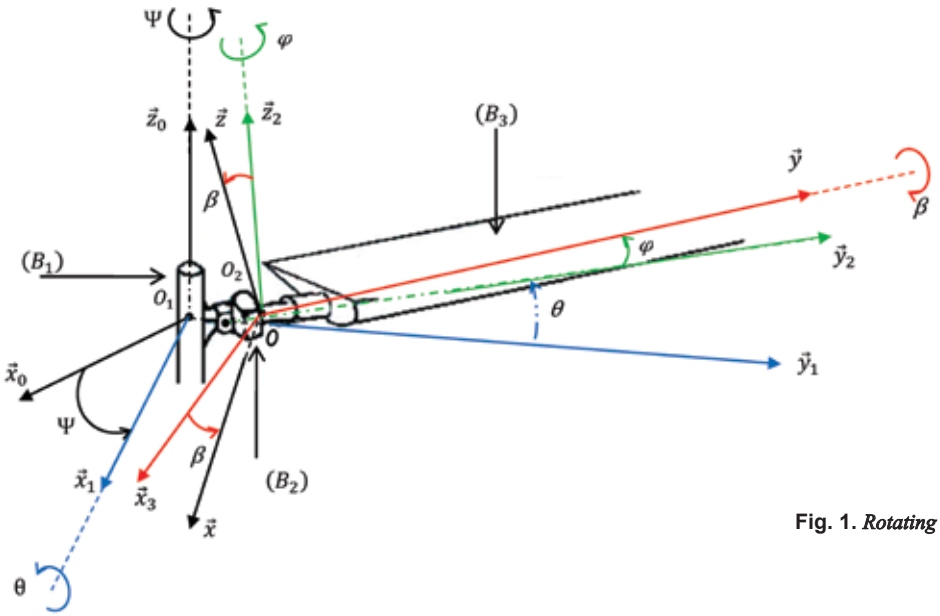

Fig. 1. *Rotating blade (OA) scheme*

Journal of Technical Science & Technologies; ISSN: 2298-0032; e-ISSN: 2346-8270; Volume 7, Issue 1, 2018

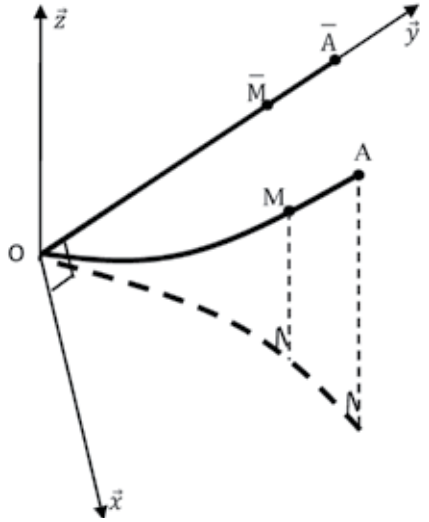

Fig. 2. *Bending of the blade (OA) in the local frame*

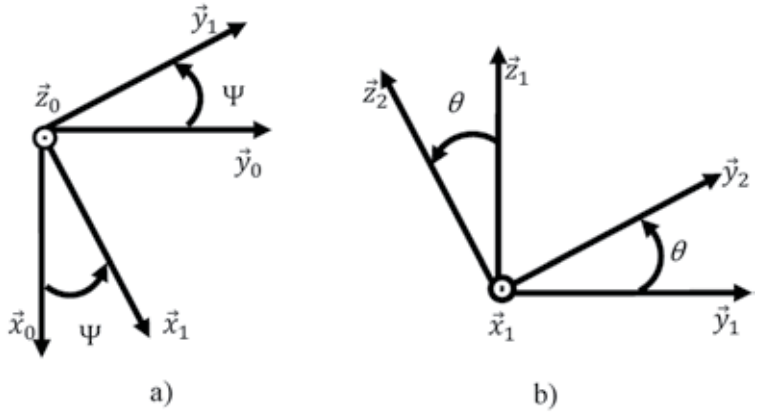

$$\vec{x}_1 = \cos\psi\vec{x}_0 + \sin\psi\vec{y}_0 \quad \vec{y}_2 = \cos\theta\vec{y}_1 + \sin\theta\vec{z}_1$$
$$\vec{y}_1 = -\sin\psi\vec{x}_0 + \cos\psi\vec{y}_0\vec{z}_2 = -\sin\theta\vec{y}_1 + \cos\theta\vec{z}_1$$

Fig. 3. *Motions of the frames – a) (R_1) and -b) (R_2)*

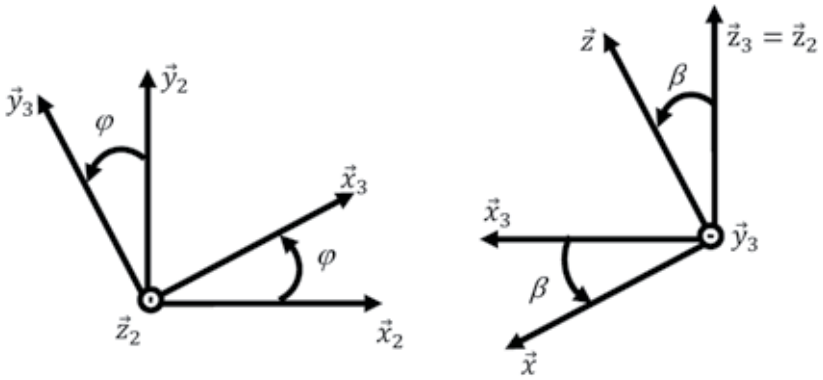

$$\vec{x}_3 = \cos\varphi\vec{x}_2 + \sin\varphi\vec{y}_2 \quad \vec{x} = \cos\beta\vec{x}_3 - \sin\beta\vec{z}_3$$
$$\vec{y}_3 = -\sin\varphi\vec{x}_2 + \cos\varphi\vec{y}_2\vec{z} = \sin\beta\vec{x}_3 + \cos\beta\vec{z}_3$$

Fig. 4. *Motions of the frames (R3) and (R)*

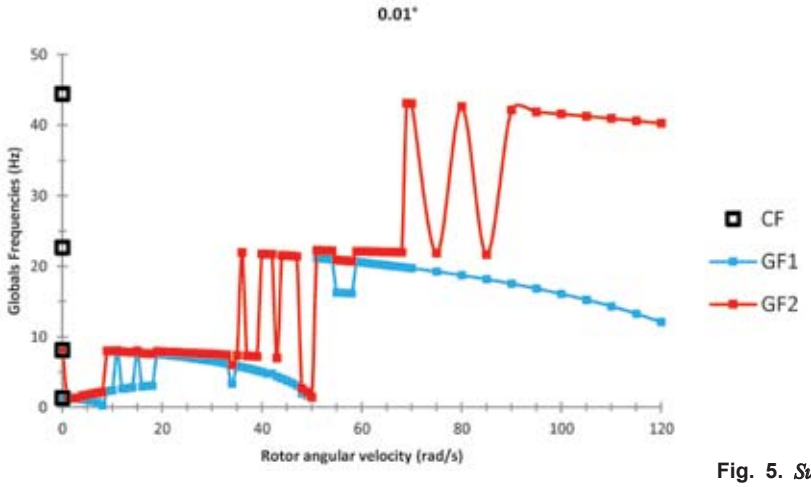

Fig. 5. *Superposition of the first two global frequencies at 0.01°*

Journal of Technical Science & Technologies; ISSN: 2298-0032; e-ISSN: 2346-8270; Volume 7, Issue 1, 2018

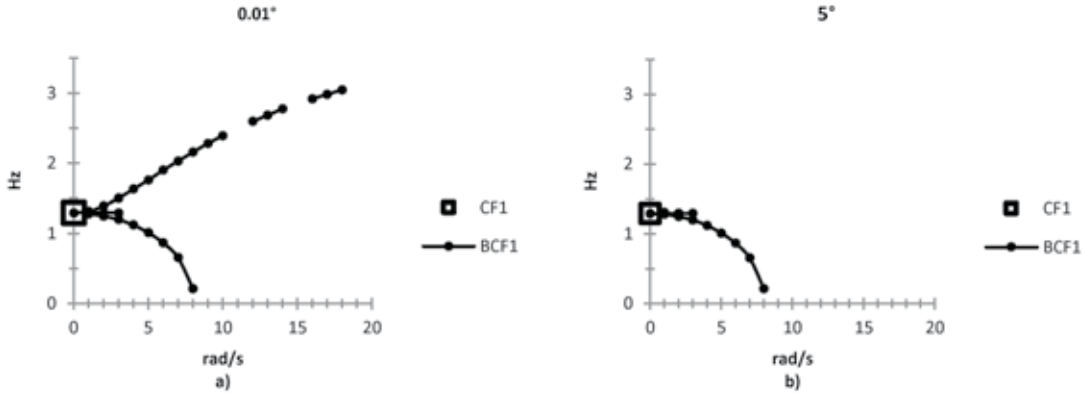

Fig. 6. *Behavior of the first cantilever frequency at -a) 0.01° and –b) 5°*

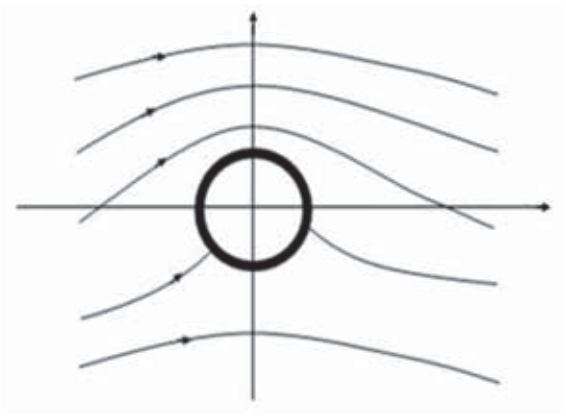

Fig. 7. *A fluid flow around a circle*

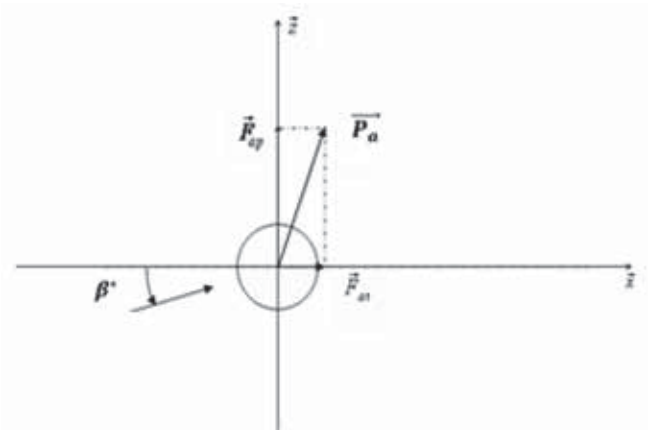

Fig. 8. *Forces exerted on a circular section*

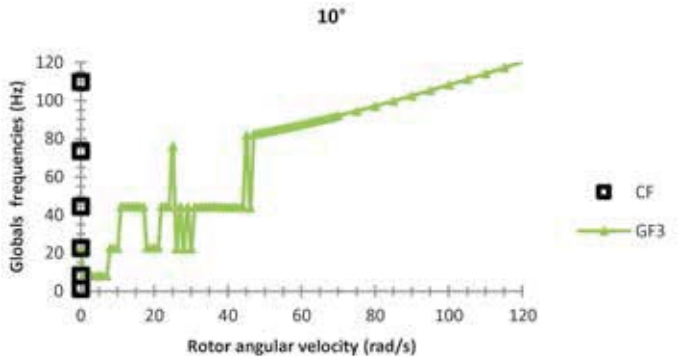

Fig. 9. *Third global frequency at β_0= 10°*

Journal of Technical Science & Technologies; ISSN: 2298-0032; e-ISSN: 2346-8270; Volume 7, Issue 1, 2018

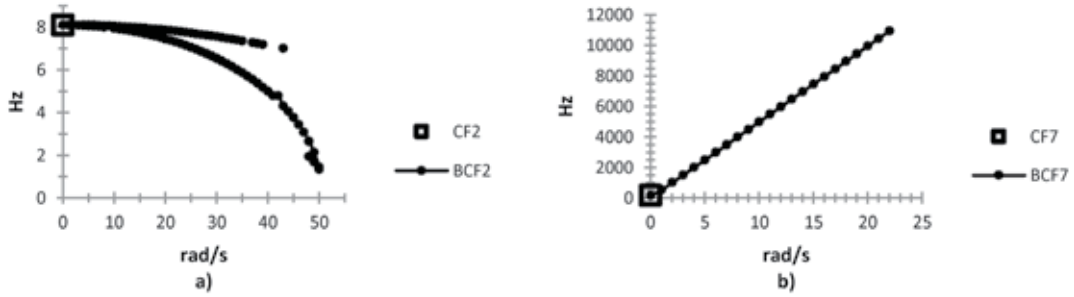

Fig. 10. *Behaviors at β_0=0,01 -a) of the 2th cantilever modes -b) of the 7th cantilever modes*